Journal Name

ARTICLE

Metal-organic frameworks assembled from flexible alicyclic carboxylate and bipyridyl ligands for sensing of nitroaromatic explosives

Xian-Dong Zhu,*[a] Yong Li,[a] Wei-Xiang Zhou,[a] Rong-Mei Liu,[a] Yu-Jie Ding,[a] Jian Lü*[b,d] and Davide M. Proserpio[c,d]

Three new metal-organic frameworks based on flexible ligands (FL-MOFs) generally formulated as [Cd(*cis*-chdc)(*anti*-bpe)(H$_2$O)]$_n$ (**1**), [Ni(*cis*-chdc)(*gauche*-bpe)]$_n$ (**2**) and [Cd$_2$(*trans*-chdc)(*cis*-chdc)(*TG*-bpp)$_2$]$_n$ (**3**) [H$_2$chdc = 1,4-cyclohexanedicarboxylic acid, bpe = 1,2-bis(4-pyridyl)ethane and bpp = 1,3-bis(4-pyridyl)propane], have been hydrothermally synthesized and characterized. Crystal structures of the three compounds feature one-dimensional infinite chains cross-linked via flexible ligand skeletons to form three-dimensional networks. Of peculiar interest, compound **1** represents a rare self-catenated MOF with 5^5·8-**zst** topology, which shows high sensitivity and quick response upon the presence of trace amount of nitroaromatic compounds. Meanwhile, the excellent ability of **1** for selective detection of 4-nitrotoluene from other nitroaromatic compounds has been demonstrated. The recyclability and reusability of **1** have also been tested based on consecutive detection reactions, in which **1** remains unchanged and detection efficiency retains.

Introduction

Nitroaromatic compounds, such as dinitrobenzene (DNB), dinitrotoluene (DNT), 2,4,6-trinitrotoluene (TNT) and 2,4,6-trinitrophenol (TNP) are the major components of high explosives. Selective and rapid detection of these chemical explosives is of immense interest owing to the ever-increasing concerns such as civilian safety, military operation and environmental management.[1] Recently, fluorescence-based detection methods based on the electron transfer and/or energy transfer mechanism have attracted increasing attention due to their high sensitivity, portability, short response time, and dual compatibility in both solid state and solution media.[2] A large number of fluorescent materials including conjugated polymers,[3] nanoparticles,[4] and metal-organic frameworks (MOFs)[5] have been employed for explosive detection. MOFs are particularly attractive for this purpose because, in principle, they are able to detect specific analytes based on structural design, thus offering good selectivity and exhibiting high density of analyte adsorption/binding sites, thereby enabling lower detection limits. Detectable change in luminescence by tuning several parameters such as porosity, surface area, and host-guest interactions makes MOFs promising candidates for sensing applications. The pioneering work of Li *et al.*, Ghosh *et al.* and other groups has demonstrated the potentials of luminescent MOFs in explosive detection.[6] Up to now, most of the reported MOF-based sensors are constructed with rigid or semi-rigid aromatic carboxylate ligands,[6-7] which can be explained by the increase of electrostatic interactions between frameworks and electron deficient nitroaromatics due to the delocalized π-electrons of ligands. Further, the photo-induced electron transfer from excited MOFs to the guest molecules results in fluorescence quenching of the MOF materials. However, using flexible carboxylate ligands as building blocks for the construction of FL-MOF[8] sensors still remains undeveloped. This is also a promising strategy to enhance the sensing ability, since the flexible frameworks could adjust their configurations to adapt to analyte molecules.[7f] On the other hand, selectivity is critical for fruitful detection in practical applications. Most of the reported MOF-based sensors exhibit highly sensitive and reversible sensing properties. However, the selective detection of specific nitroaromatic explosive from a mixture of others (with different numbers of –NO$_2$ groups) has rarely been reported.[6g, 7h-k]

Based on the above considerations, we have selected 1,4-cyclohexanedicarboxylic acid (H$_2$chdc) as a primary ligand coupled to auxiliary ligands, 1,2-bis(4-pyridyl)ethane (bpe) and 1,3-bis(4-pyridyl)propane (bpp), to construct new FL-MOFs by the adjustment of metal nodes with various connection modes. In this contribution, we report the preparation and crystal structures of three FL-MOFs

a. *School of Biological & Chemical Engineering, Anhui Polytechnic University, Wuhu 241000, P. R. China, E-mail: zhuxd@ahpu.edu.cn.*
b. *Fujian Provincial Key Laboratory of Soil Environmental Health and Regulation, College of Resources and Environment, Fujian Agriculture and Forestry University, Fuzhou 350002, P. R. China, E-mail: lujian05@yeah.net.*
c. *Dipartimento di Chimica, Università degli Studi di Milano, Milano 20133, Italy.*
d. *Samara Center for Theoretical Materials Science (SCTMS), Samara National Research University, Samara 443086, Russia.*

formulated as [Cd(*cis*-chdc)(*anti*-bpe)(H_2O)]$_n$ (**1**), [Ni(*cis*-chdc)(*gauche*-bpe)]$_n$ (**2**), and [Cd$_2$(*trans*-chdc)(*cis*-chdc)(*TG*-bpp)$_2$]$_n$ (**3**), which feature one-dimensional infinite chains further cross-linked via flexible ligand skeletons to form three-dimensional networks. The difference in ligand conformations plays an important role on FL-MOF architectures reflected by the unique structural features of all three compounds. Of peculiar interest, compound **1** represents a rare self-catenated MOF with $6^5 \cdot 8$-**zst** topology, which shows high sensitivity and quick response to trace amount of nitroaromatic compounds present.

Experimental

Materials and general methods

All commercially available reagents and starting materials were of reagent-grade quality and used without further purification. Microwave-assisted syntheses were carried out in a microwave oven (XH-800S-10, 0-1200W, Beijing Xianghu Corp.). UV-Vis absorption spectra were measured using a Jingke L6S spectrometer. Elemental analyses (C, H, N) were carried out on an Elementar Vario EL III analyzer. Powder X-ray diffraction (PXRD) data were collected on a Bruker D8 ADVANCE diffractometer with Cu-Kα radiation (λ = 1.5418 Å). Fourier transform infrared (FT-IR) spectra were recorded on PerkinElmer Spectrum One with KBr pellets in the range 4000-400 cm^{-1}. Thermogravimetric analysis (TGA) was performed under nitrogen atmosphere with a heating rate of 10 °C min^{-1} using an NETZSCH STA 449C unit.

Synthesis of compound [Cd(*cis*-chdc)(*anti*-bpe)(H_2O)]$_n$ (1)

As a typical synthetic procedure, a mixture of Cd(NO$_3$)$_2 \cdot$4H$_2$O (0.030 g, 0.1 mmol), H$_2$chdc (0.017 g, 0.1 mmol), bpe (0.019 g, 0.1 mmol), NaOH (0.004g, 0.1 mmol) and 10 ml distilled water was sealed in a 25ml Teflon-lined stainless steel autoclave, and heated at 160 $^{\circ}$C for 72 hours, then cooled naturally to room temperature. Colourless block crystals of **1** were collected by filtration, washed with distilled water, and dried in air at ambient temperature. Yield: 36% (based on Cd). Calcd for C$_{20}$H$_{24}$N$_2$O$_5$Cd (484.82): C 49.55, H 4.99, N 5.78; found: C 48.93, H 4.90, N 5.66. IR (KBr, cm^{-1}): 3413 (s, br), 2913 (m), 2856 (w), 1610 (s), 1550 (vs), 1417 (s), 1014 (m), 837 (m), 547 (m).

Synthesis of compound [Ni(*cis*-chdc)(*gauche*-bpe)]$_n$ (2)

Compound **2** was synthesized with a same recipe as that of **1**, using Ni(NO$_3$)$_2 \cdot$6H$_2$O (0.029 g, 0.1 mmol) instead of Cd(NO$_3$)$_2 \cdot$4H$_2$O. Green block crystals of **2** were collected by filtration, washed with distilled water, and dried in air at ambient temperature. Yield: 52% (based on Ni). Calcd for C$_{20}$H$_{22}$N$_2$O$_4$Ni (413.09): C 58.15, H 5.37, N 6.78; found: C 57.85, H 5.28, N 6.72. IR (KBr, cm^{-1}): 3436 (m, br), 3050 (m), 2937 (s), 2867 (w), 1610 (vs), 1535 (vs), 1430 (s), 1222 (m), 1025(m), 931(w), 817 (m), 557 (m).

Synthesis of compound [Cd$_2$(*trans*-chdc)(*cis*-chdc)(*TG*-bpp)$_2$]$_n$ (3)

Compound **3** was synthesized with a similar procedure as that of **1**, using less amount of NaOH (0.001g, 0.025 mmol) at lower temperature of 130 $^{\circ}$C. Colourless block crystals of **3** were collected by filtration, washed with distilled water, and dried in air at ambient temperature. Yield: 52% (based on Cd). Calcd for C$_{21}$H$_{24}$N$_2$O$_4$Cd (480.84): C 52.45, H 5.03, N 5.82; found: C 52.31, H 4.72, N 5.37. IR (KBr, cm^{-1}): 3469 (s, br), 2919 (m), 2859 (w), 1610 (s), 1573 (vs), 1411 (s), 1018 (m), 817 (m).

X-ray crystallographic study

Data collection for **1**-**3** was performed on a Rigaku Mercury 2 CCD diffractometer equipped with graphite-monochromated Mo-Kα radiation (λ = 0.71073 Å) at room temperature. Both data sets were corrected for Lorentz and polarization factors as well as for absorption by a multiscan method.[9] The structures were solved by direct methods and refined by the full-matrix least-squares on F^2 using the *SHELXTL-97* program.[10] All non-hydrogen atoms were treated anisotropically. The positions of hydrogen atoms attached to carbon atoms were generated geometrically. Idealized positions of hydrogen atoms of water molecules were located from Fourier difference maps and refined isotropically. The date set of compound **1** shows a Flack parameter of 0.56(3) that indicate the existence of racemic twinning. This is supported by the refinements of several data sets collected on different crystals. We have also tried to solve this structure in the centrosymmetric space group *Pnma*, but R_1 (about 0.169) is too high and many atoms have ADP nonpositive-definite. Therefore, we finally chose space group *Pna*2$_1$, which gave a satisfactory refinement with R_1 = 0.0237 for 4214 unique reflections with *I* > *2σ* (*I*). Compound **3** has disorder about the dipyridyl ligand that was modeled successfully via the PART and ISOR commands to restrain the carbon atoms at appropriate bond lengths. Crystallographic data and structure refinements for **1**-**3** are listed in Table S1.

Fluorescence sensing measurement

The photoluminescence excitation and emission spectra of compounds **1**-**3** were recorded on a Hitachi F-4500 spectrophotometer. The emission lifetimes were measured on an Edinburgh FLS-920 fluorescence spectrometer. The fluorescence properties of the sample in solid state and various solvent suspensions were examined at room temperature. The **1**-solvent suspensions were prepared by introducing 20 mg fine grinding sample of **1** immersed in different organic solvents (20 mL), treated by ultrasonication for 30 minutes, and then aged for 24 hours to form stable emulsions. In typical fluorescence quenching experimental setup, 2 mL suspension of **1** in DMF was placed in a 1 cm quartz cuvette and the fluorescence response upon excitation at 290 nm was measured in situ after incremental addition of freshly prepared 20 mM analyte solution in DMF in the range of 320-550 nm.

Results and discussion

Syntheses

Compounds **1**-**3** were synthesized under hydrothermal conditions. Interestingly, the cadmium compounds **1** and **3** could also be synthesized by microwave-assisted hydrothermal reactions at similar temperatures (160 $^{\circ}$C and 130 $^{\circ}$C) but significantly short

time (15 minutes versus 3 days) to the conventional syntheses in comparable yields. In this context, microwave heating is more efficient and less of an energy consumer. Unfortunately, attempt to synthesize compound **2** by microwave-assisted hydrothermal reaction was failed. The experimental powder X-ray diffraction patterns of compounds **1**-**3** match well with the ones simulated from single crystal data, suggesting the phase purity of the products (Fig. S1-3). All carboxylate groups of H_2chdc in **1**-**3** are found deprotonated as evidenced by FT-IR spectral data (Fig. S4-6). Although the three compounds were synthesized under similar conditions, there are great differences in ligand conformations, which exert an important influence on FL-MOF architectures reflected by the unique structural features of compounds **1**-**3** as described below.

Crystal structural description

Single crystal X-ray diffraction analysis indicates that the compound **1** crystallizes in non-centrosymmetric space group *Pna*2_1. The asymmetric unit contains one crystallographically independent Cd^{2+} ion, one deprotonated $chdc^{2-}$ anion, one bpe ligand, and one coordinated water molecule. As shown in Fig. S7, the Cd1 atom is hepta-coordinated and can be described as distorted pentagonal bipyramid geometry. Two pairs of chelating carboxylate oxygen donors from different $chdc^{2-}$ ligands and one water molecules comprise the equatorial plane; two pyridyl nitrogen donors from two bpe ligands occupy the remaining axial sites [N1-Cd1-N2A = 165.611(1) °]. The Cd–O(N) distances are in the range of 2.353(3) to 2.491(3) Å, and the O(N)–Cd–O(N) angles vary from 53.63(9) to 167.92(8) °.

It is worthy to note that only one kind of *cis*-conformation of the $chdc^{2-}$ ligand is present in the structure, even though the H_2chdc starting material contains both *cis*- and *trans*-conformation.[11] Both carboxylate groups of the *cis*-$chdc^{2-}$ ligand exhibit bidentate chelating mode to Cd^{2+} centers. The bpe ligand adopts *anti*-configuration with the N···N distance of *ca.* 9.33 Å, acting as a bidentate bridging ligand in compound **1**. Based on aforementioned coordination modes, two Cd^{2+} ions are bridged by carboxylate groups of *cis*-$chdc^{2-}$ ligand to afford the repeating dinuclear units and extend into an infinite 2_1 helical chain along the *c* axis. The adjacent chains are connected together by *anti*-bpe ligands into two-dimensional distorted honeycomb (**hcb**) layers in which parallel left- and right-handed chains alternate (Fig. 1a). The neighboring layers are further cross-linked *via anti*-bpe ligands, and give rise to a three-dimensional framework (Fig. 1b). Since the right- and left-handed helices are alternately arranged, the overall network, therefore, is achiral. By means of topological analysis using *ToposPro*,[12] the network can be simplified by considering cadmium atoms as 4-coordinated nodes, $chdc^{2-}$ and bpe ligands as linkers, which give rise to a 4-c uninodal net with $6^5 \cdot 8$-**zst** topology (Fig. 1b and 1c). The **zst** net has been rarely recognized in coordination polymer compounds and metal-organic frameworks with only five know examples, all with mixed ligands[13] as collected into ToposPro TTD database.[14] The **zst** net with vertex symbol $[6.6.6.6.6_2.10_{12}]$ shows also the property of self-catenation of the 10-rings (Fig. 1c).[15]
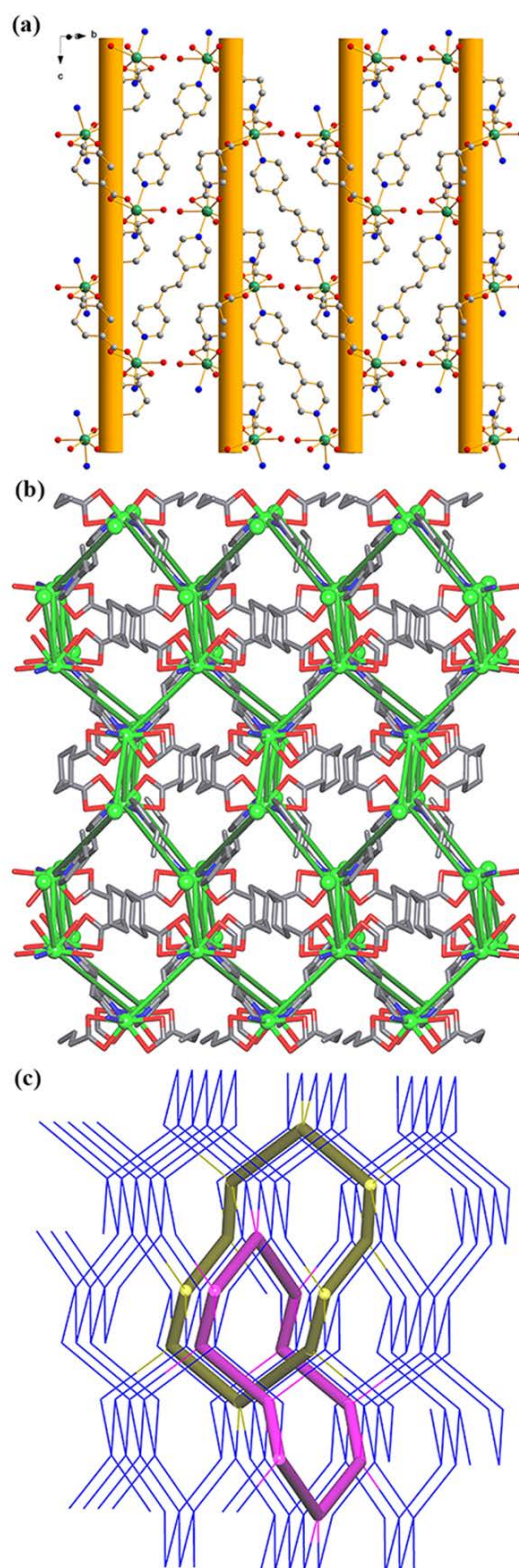

Fig. 1 (a) View of the two-dimensional helical structure of 1. (b) Perspective view of three-dimensional framework of 1 along the c axis with the underlying net in green. (c) The underlying net $6^5 \cdot 8$-**zst** showing the self-catenation of 10-rings.
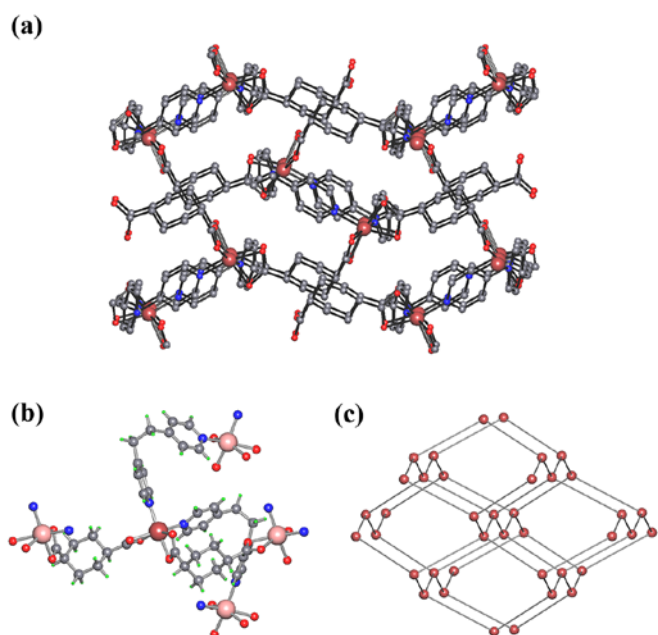
Fig. 2 (a) The 3D packing diagram of compound **2**. (b) A view of the linking fashion of nickel centres. (c) Topological presentation of the 6^6-**dia** net.

Compound **2** crystallizes in the orthorhombic space group $Pna2_1$. The asymmetric unit of **2** contains one crystallographic independent Ni^{2+} ion, one chdc^{2-} anion, and one bpe ligand. As illustrated in Fig. S8, Each Ni^{2+} ion is hexa-coordinated to four carboxylate oxygen atoms associated with two chdc^{2-} ligands and two pyridyl nitrogen atoms from different bpe ligands, exhibiting distorted octahedral coordination geometry. The Ni–O(N) bond lengths are in the range of 2.044(4) to 2.113(3) Å, and the O(N)–Ni–O(N) bond angles vary from 62.94(13) to 167.06(15)°. The chdc^{2-} ligand adopts *cis*-configuration with bidentate chelating coordination mode. It is interesting to find different configuration of *gauche*-bpe ligand with the N···N distance of *ca.* 5.96 Å compared to compound **1**. In the polymeric structure of **2**, the Ni^{2+} ions are connected by carboxylate groups of *cis*-chdc^{2-} ligands to form an infinite zigzag chain along the *a* axis. The one-dimensional infinite chains are further cross-linked via the bridging *gauche*-bpe ligands in two different directions, to form a three-dimensional network (Fig. 2a). By means of topological analysis using *ToposPro*,[12] the network can be simplified by considering nickel atoms as 4-coordinated nodes, chdc^{2-} and bpe ligands as linkers, which give rise to a **dia** net, the most frequent 4-c uninodal net (Fig. 2b and 2c). **dia** nets have been reported only for two other coordination networks with chdc^{2-} together with long rigid ligands that results in interpenetration.[16] In **2** the flexible bpe ligands hamper interpenetration.
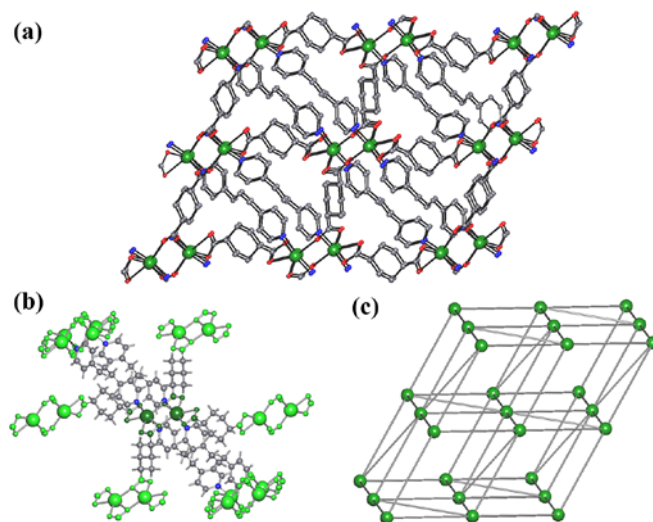

Fig. 3 (a) The 3D packing diagram of compound **3**. (b) A view of the linking fashion of dinuclear cadmium clusters. (c) Topological presentation of the **sqc117** net.

Compound **3** crystallizes in the triclinic space group P-1. The asymmetric unit of **3** is composed of two crystallographically independent Cd^{2+} ions, two chdc^{2-} anions, and two bpp ligands. As illustrated in Fig. S9, each Cd^{2+} ion is hexa-coordinated to four carboxylate oxygen atoms associated with three chdc^{2-} ligands and two pyridyl nitrogen atoms from different bpp ligands, exhibiting distorted octahedral coordination geometry. The Cd–O(N) bond lengths are in the range of 2.214(13) to 2.458(12) Å, and the O(N)–Cd–O(N) bond angles vary from 53.6(3) to 173.3(4)°. Interestingly, two different conformational isomers of *cis*-chdc^{2-} and *trans*-chdc^{2-} in the building unit of **3** adopt μ_4-$(\kappa^1$-$\kappa^1)$-$(\kappa^1$-$\kappa^1)$ and μ_2-κ^2:κ^2 binding modes, respectively. The bpp ligand adopts *TG*-configuration with the N···N distance of *ca.* 9.08 and 8.94 Å, acting as a bidentate bridging ligand. Based on the above mentioned coordination modes, two independent Cd^{2+} ions are bridged together by *cis*-chdc^{2-} ligand, giving a Cd···Cd distance of 4.05 and 4.48 Å and extending the structure into one-dimensional infinite chain. The adjacent chains are further connected by *trans*-chdc^{2-} and *TG*-bpp ligands in different directions, giving rise to an overall three-dimensional structure (Fig. 3a). By means of topological analysis using *ToposPro*,[12] the network can be simplified by considering dinuclear cadmium clusters as 6-coordinated nodes, chdc^{2-} and bpp ligands as linkers, which give rise to a 8-c uninodal net with **sqc117** topology (Fig. 3b and 3c).[17] Compound 3 is isoreticular with [Co$_2$(*trans*-chdc)(*cis*-chdc)(*TG*-bpp)$_2$]$_n$ [11a] and the underlying net **sqc117** has been observed also in seven other coordination networks containing multinuclear nodes.[18]

Photoluminescence property

The photoluminescence behaviours of compounds **1**-**3** as well as the free ligands were examined in the solid state at room temperature. As shown in Fig. 4a, compound **1** exhibits strong emission at 372 nm with a shoulder band at 358 nm (λ_{ex} = 290 nm), while relatively weak luminescence was observed at 376 nm for bpe (λ_{ex} = 290 nm) and at 339 and 431 nm for H$_2$chdc (λ_{ex} = 280 nm) at the same experimental conditions. The luminescence of **1** can be

tentatively assigned to the intraligand transition of bpe ligand, since the similar emission was observed for the ligand.[19] The photoluminescence spectra of **1** dispersed in different solvents also exhibit strong emission at 372 nm upon excitation at 290 nm (Fig. 4b). Interestingly, its emission is largely dependent on the solvent molecules, particularly in the case of acetone, which exhibited the most significant quenching effects (Fig. 4c). Compound **2** do not emit light, while relatively weak luminescence has been observed at 391 nm (λ_{ex} = 330 nm) for **3** at the same experimental conditions compared to **1**. The red-shifted emission band at 391 nm (λ_{ex} = 330 nm) of **3**, compared with the band at 376 nm (λ_{ex} = 300 nm) of bpp, was probably related to the intraligand fluorescent emission (Fig. S10). Due to the weak photoluminescence of compounds **2** and **3**, only the photoluminescent sensing property of compound **1** was studied, as detailed below.

Detection for nitroaromatic compounds

Taking the above photoluminescence study into consideration, exploration of the potential sensing ability of compound **1** towards nitroaromatic explosives is possible. The fluorescence-quenching titrations have been carried out with the DMF suspension of **1** by gradual addition of different concentrations of 4-nitrotoluene (4-NT), nitrobenzene (NB), 1,3-dinitrobenzene (1,3-DNB), 2,4-dinitrotoluene (2,4-DNT), 2,6-dinitrotoluene (2,6-DNT) and 2,4,6-trinitrotoluene (TNT) (Fig. 5a and Fig. S11-15). The quenching efficiencies were estimated by using the formula $(1 - I/I_0) \times 100\%$, where I_0 and I are the fluorescence intensities before and after the addition of nitroaromatic compounds. As shown in Fig. 5b, the maximum fluorescence intensity of **1** was reduced by 78.1, 52.7, 48.7, 46.0, 45.8 and 43.2 % upon exposure to 0.3 mM concentration of 4-NT, 2,4-DNT, NB, TNT, 1,3-DNB and 2,6-DNT respectively. When the concentration of 4-NT increased to 0.5 mM, the bright blue luminescence of the suspension observed under UV-light disappeared, with 90.3% quenching efficiency. Incremental addition of 4-NT exhibited a significant quenching effect on the fluorescence intensity of the dispersed **1** in DMF, whereas NB, 1,3-DNB, 2,4-DNT, 2,6-DNT and TNT showed a minor quenching effect (Fig. 5c). To verify the fluorescence response of **1** towards other aromatic substituents, the sensing experiments were also performed with benzene, toluene, p-xylene, chlorobenzene and phenol but negligible quenching effect was observed (Fig. S16-20). The significant quenching effect of 4-NT on fluorescence intensity of **1** indicates the potential of **1** for sensing of trace amount of nitroaromatic compounds.
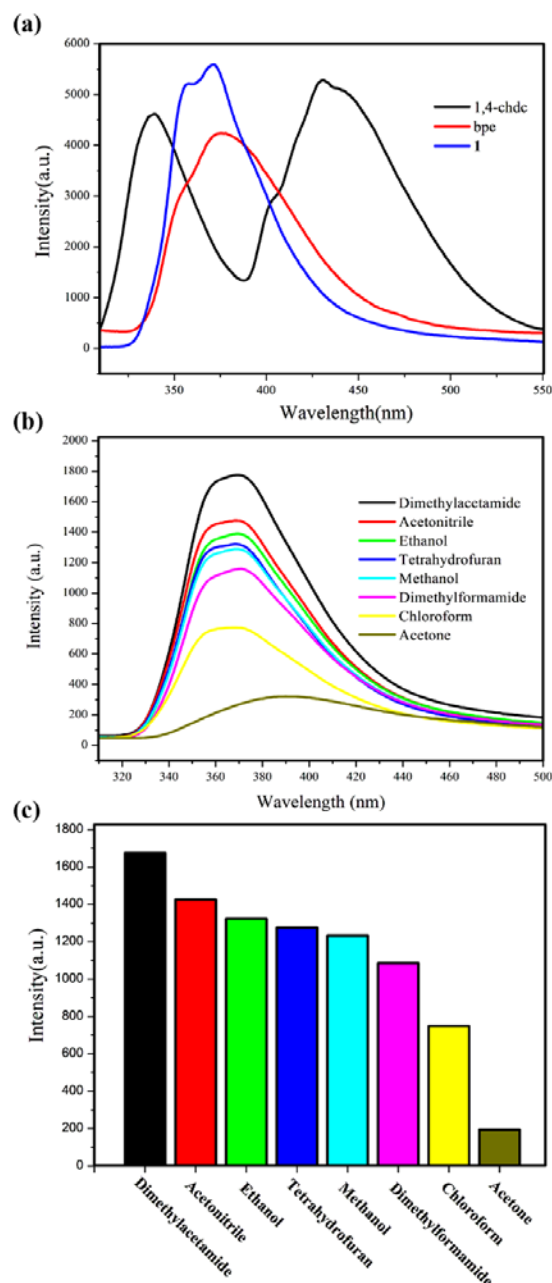

Fig. 4 (a) Solid-state emission spectrum for free ligands and compound **1**. (b) Emission spectrum of **1** dispersed in different solvents. (c) Fluorescence intensity ratio histograms of **1** dispersed in different solvents.

To investigate the quenching mechanism between the sensing material and analytes, the fluorescence quenching efficiency was further analyzed using the Stern–Volmer (S-V) equation, $(I_0/I) = K_{sv}[Q]+1$, where I_0 and I are the fluorescence intensities before and after the addition of nitroaromatic explosives, $[Q]$ is the molar concentration of analytes, and K_{sv} is the quenching constant (M^{-1}). From the linear fitting of the S–V plots (Fig. 6a), the calculated K_{sv} values for 4-NT was found to be 2.64×10^4 M^{-1} which indicates the super quenching ability of **1** toward 4-NT. The calculated K_{sv} values for NB, 1,3-DNB, 2,4-DNT, 2,6-DNT and TNT were 5.04×10^3, 4.43×10^3, 6.21×10^3, 3.87×10^3 and 3.10×10^3 M^{-1}, respectively, which

lie in the normal range for the known luminescent metal–organic frameworks.[6-7] If only one kind of quenching mechanism is operative, whether static or dynamic, the quenching can be represented by the Stern–Volmer equation and the I_0/I versus $[Q]$ plot should be linear. To better understand the mechanism of sensing, the variation of the fluorescence lifetime of **1** was checked in the absence and presence of 4-NT (Fig. 6b). The emission lifetime of **1** showed a single exponential feature with $\tau_0 = 0.39$ ns and remained essentially unchanged by addition of 4-NT suggesting the quenching process follows static mechanism. The UV-vis spectra of **1** upon incremental addition of 4-NT were recorded (Fig. 6c). The absorption band intensity at 242 nm reduced rapidly with increased 4-NT concentration, indicating a strong interaction between the sensing material and the 4-NT at ground state. Notably, upon gradual addition a new absorption band at 302 nm was appeared which confirms the absorption by 4-NT is the main source for the observed fluorescence quenching.

To examine the potential of the selective sensing behavior of **1** towards 4-NT in presence of other interfering nitroaromatic analytes, a series of competition experiments were performed by gradual addition of a solution of different nitroaromatic analogues followed by 4-NT into **1**, and the corresponding fluorescence spectra were monitored. As shown in Fig. S21-25, the initial addition of different analytes showed negligible effect on the luminescent intensity of **1**, but a significant fluorescence quenching occurred after the incremental addition of 4-NT to the mixed emulsion. The stepwise decrease in luminescent intensity demonstrates the high ability of **1** for selectively detecting 4-NT even in the presence of other nitroaromatic compounds.

It is noteworthy that no pre-activation process was carried out before the sensing experiments, which shows the operability advantage of **1** over other reported MOF-based sensors (need the evacuation of coordinated or guest solvent molecules). Also, the detection ability of **1** could be regenerated from emulsion and reused by simply filtrating and washing several times with DMF. As shown in Fig. S26, the initial fluorescence intensity of the recovered material shows no obvious decrease over five repeated cycles, which implies a high photostability of **1** for its long-time nitroaromatic compounds detection application. The PXRD patterns of the initial sample and recovered sample after five cycles of quenching and recovery also indicate the high stability of this compound (Fig. S27).
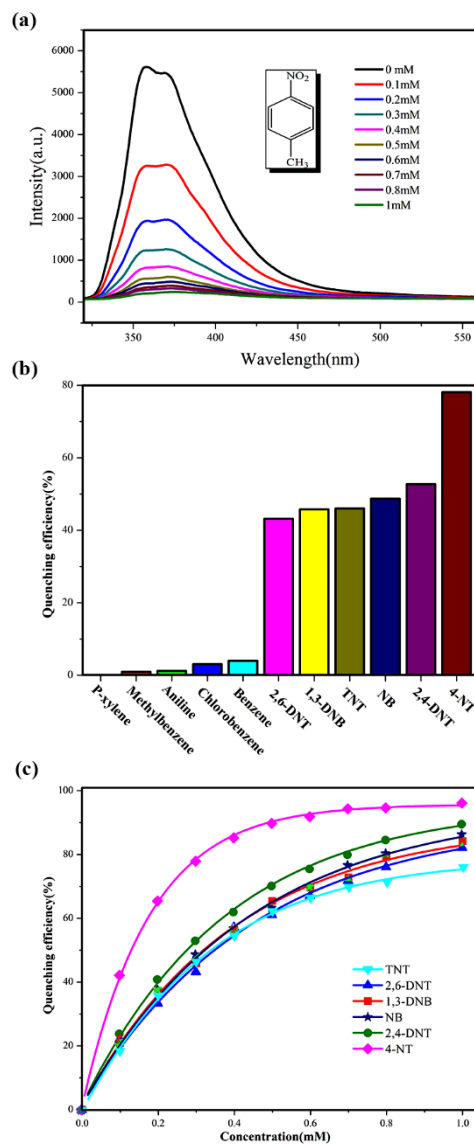

Fig. 5 (a) Fluorescence titration of **1** upon incremental addition of 4-NT solution in DMF. (b) Fluorescence intensity ratio histograms of **1** upon exposure to 0.3 mM concentration of different analytes. (c) Plot of quenching efficiency of **1** dispersed in DMF with different analytes.
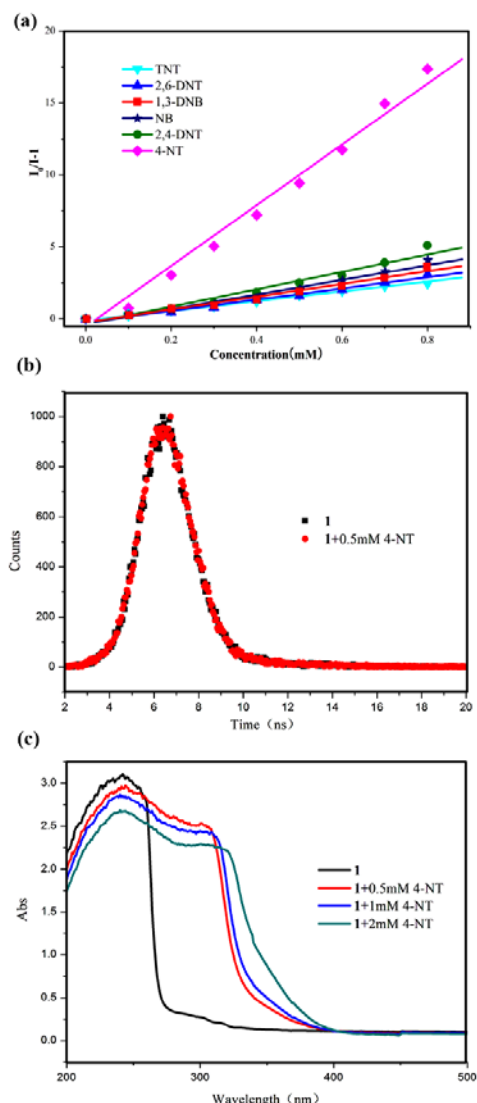
Fig. 6 (a) Stern-Volmer plots of **1** dispersed in DMF with different analytes. (b) Fluorescence decay profile of **1** before and after addition of 4-NT. (c) Adsorption spectra of **1** in DMF upon incremental addition of 4-NT.

Conclusions

In summary, three new FL-MOFs generally formulated as [Cd(*cis*-chdc)(*anti*-bpe)(H$_2$O)]$_n$ (**1**), [Ni(*cis*-chdc)(*gauche*-bpe)]$_n$ (**2**) and [Cd$_2$(*trans*-chdc)(*cis*-chdc)(*TG*-bpp)$_2$]$_n$ (**3**) have been successfully synthesized under hydrothermal conditions. The crystal structures of all three compounds feature one-dimensional infinite chains further cross-linked via flexible ligands to form three-dimensional networks. Of peculiar interest, compound **1** represents a rare self-catenated MOF with 6^5·8-**zst** topology, which shows high sensitivity and quick response upon the presence of trace amount of nitroaromatic compounds. Meanwhile, the excellent ability of **1** for selective detection of 4-nitrotoluene from other nitroaromatic compounds has been demonstrated. The recyclability and reusability of **1** have also been tested based on consecutive detection reactions, in which **1** remains unchanged and detection efficiency sustained. Compound **1** is one of the few luminescent

sensors based on FL-MOFs that exhibit highly sensitive, reversible sensing, and selective detection of nitroaromatic explosives. This study extends the applications of FL-MOFs as promising materials for versatile chemical sensors.

Acknowledgements

Notes and references

1 (a) J. Yinon in Forensic and Environmental Detection of Explosives, John Wiley & Sons, Chichester, 1999; (b) W. C. Trogler in NATO ASI Workshop, Electronic Noses & Sensors for the Detection of Explosives, Kluwer Academic Publishers, Dordrecht, 2004.

2 (a) M. E. Germain and M. J. Knapp, *Chem. Soc. Rev.* 2009, **38**, 2543; (b) Y. Salinas, M. R. Martinez, M. D. Marcos, F. Sancenon, A. M. Castero, M. Parra and S. Gil, *Chem. Soc. Rev.* 2012, **41**, 1261.

3 (a) S. W. Thomas, G. D. Joly and T. M. Swager, *Chem. Rev.*, 2007, **107**, 1339; (b) H. Cavaye, P. E. Shaw, X. Wang, P. L. Burn, S.-C. Lo and P. Meredith, *Macromolecules*, 2010, **43**, 10253; (c) K. K. Kartha, S. S. Babu, S. Srinivasan and A. Ajayaghosh, *J. Am. Chem. Soc.* 2012, **134**, 4834.

4 (a) E. S. Snow, F. K. Perkins, E. J. Houser, S. C. Badescu and T. L. Reinecke, *Science*, 2005, **307**, 1942; (b) M. E. Kose, B. A. Harruff, Y. Lin, L. M. Veca, F. S. Lu and Y. P. Sun, *J. Phys. Chem. B*, 2006, **110**, 14032.

5 (a) Y. Cui, Y. Yue, G. Qian and B. Chen, *Chem. Rev.*, 2012, **112**, 1126; (b) L. E. Kreno, K. Leong, O. K. Farha, M. Allendorf, R. P. Van Duyne and J. T. Hupp, *Chem. Rev.*, 2012, **112**, 1105; (c) Y. Cui, B. Chen and G. Qian, *Coord. Chem. Rev.*, 2014, **76**, 273; (d) Z. Hu, B. J. Deibert and J. Li, *Chem. Soc. Rev.*, 2014, **43**, 5815.

6 (a) A. Lan, K. Li, H. Wu, D. H. Olson, T. J. Emge, W. Ki, M. Hong and J. Li, *Angew. Chem., Int. Ed.*, 2009, **48**, 2334; (b) Z. Zhang, S. Xiang, S. Rao, Q. Zheng, F. R. Fronczek, G. Qian and B. Chen, *Chem. Commun.*, 2011, **47**, 7205; (c) S. Pramanik, C. Zheng, X. Zhang, T. J. Emge and J. Li, *J. Am. Chem. Soc.*, 2011, **133**, 4153; (d) C. Zhang, Y. Che, Z. Zhang, X. Yang and L. Zang, *Chem. Commun.*, 2011, **47**, 2336; (e) B. Gole, A. K. Bar and P. S. Mukherjee, *Chem. Commun.*, 2011, **47**, 12137; (f) M. Guo and Z. M. Sun, *J. Mater. Chem.*, 2012, **22**, 15939; (g) S. S. Nagarkar, B. Joarder, A. K. Chaudhari, S. Mukherjee and S. K. Ghosh, *Angew. Chem., Int. Ed.*, 2013, **52**, 2881.

7 (a) D. Ma, B. Li, X. Zhou, Q. Zhou, K. Liu, G. Zeng, G. Li, Z. Shi and S. Feng, *Chem. Commun.*, 2013, **49**, 8964; (b) G. Wang, L. Yang, Y. Li, H. Song, W. Ruan, Z. Chang and X. Bu, *Dalton Trans.*, 2013, **42**, 12865; (c) Q. Zhang, A. Geng, H. Zhang, F. Hu, Z. Lu, D. Sun, X. Wei and C. Ma, *Chem. Eur. J.*, 2014, **20**, 4885; (d) B. Gole, A. K. Bar and P. S. Mukherjee, *Chem. Eur. J.*, 2014, **20**, 13321; (e) D. Tian, Y. Li, R. Chen, Z. Chang, G. Wang and X. Bu, *J. Mater. Chem. A*, 2014, **2**, 1465; (f) G. Wang, C. Song, D. Kong, W. Ruan, Z. Chang and Y. Li, *J. Mater. Chem. A.*, 2014, **2**, 2213; (g) D. Singh and C. M. Nagaraja, *Dalton Trans.*, 2014, **43**, 17912; (h) K. S. Asha, K. Bhattacharyya and

S. Mandal, *J. Mater. Chem. C.*, 2014, **2**, 10073; (i) S. Sanda, S. Parshamoni, S. Biswasa and S. Konar, *Chem. Commun.*, 2015, **51**, 6576; (j) J. Ye, L. Zhao, R. F. Bogale, Y. Gao, X. Wang, X. Qian, S. Guo, J. Zhao and G. Ning, *Chem. Eur. J.*, 2015, **21**, 2029; (k) C. Zhang, L. Sun, Y. Yan, J. Li, X. Song, Y. Liu and Z. Liang, *Dalton Trans.*, 2015, **44**, 230.

8   (a) Z. Lin and M.-L. Tong, *Coord. Chem. Rev.*, 2011, **255**, 421; (b) Z. Lin, J. Lu, M. Hong and R. Cao, *Chem. Soc. Rev.*, 2014, **43**, 5867; (c) X. Zhu, J. Lü, X. Li, S. Gao, G. Li, F. Xiao and R. Cao, *Cryst. Growth Des.*, 2008, **8**, 1897-1901; (d) X. Zhu, Z. Lin, T. Liu, B. Xu and R. Cao, *Cryst. Growth Des.*, 2012, **12**, 4708.

9   *CrystalClear*, version 1.3.5; Rigaku Corp.: Woodlands, TX, 1999.

10 G. M. Sheldrick, *SHELXTL*, Crystallographic Software Package, version 5.1; Bruker-AXS: Madison, WI, 1998.

11 (a) S.-C. Hsu, P.-S. Chiang, H.-K. Liu, S.-H. Lo and C.-H. Lin, *J. Chin. Chem. Soc.*, 2012, **59**, 18; (b) X. Wang, W. Yao, Y.-F. Qi, M.-F. Luo, Y.-H. Wang, H.-W. Xie, Y. Yu, R.-Y. Ma and Y.-G. Li, *CrystEngComm*, 2011, **13**, 2542.

12 V. A. Blatov, A. P. Shevchenko and D. M. Proserpio, *Cryst. Growth Des.*, 2014, **14**, 3576-3586; see also http://www.topospro.com.

13 (a) FISZIR: Q. Chang, X.-R. Meng, Y.-L. Song and H.-W. Hou, *Inorg. Chim. Acta*, 2005, **358**, 2117; (b) ALIGOS: S.-T. Zheng, Y. Li, T. Wu, R. A. Nieto, P. Feng and X. Bu, *Chem. Eur. J.*, 2010, **16**, 13035; (c) YIGZIZ, YIGZOF, YIGZUL: G.-Z. Liu, S.-H. Li, X.-L. Li, L.-Y. Xin and L.-Y. Wang, *CrystEngComm*, 2013, **15**, 4571.

14 E. V. Alexandrov, V. A. Blatov, A. V. Kochetkov and D. M. Proserpio, *CrystEngComm*, 2011, **13**, 3947.

15 (a) L. Carlucci, G. Ciani and D. M. Proserpio, *Coord. Chem. Rev.*, 2003, **246**, 247; (b) V. A. Blatov, M. O'Keeffe and D. M. Proserpio, *CrystEngComm*, 2010, **12**, 44.

16 (a) ZAWNUI: S.-S. Chen, Y. Zhao, J. Fan, T. Okamura, Z.-S. Bai, Z.-H. Chen, W.-Y. Sun, *CrystEngComm*, 2012, **14**, 3564-3576; (b) KINHAS: Z.-Q. Shi, Y.-Z. Li, Z.-J. Guo, H.-G. Zheng, *Cryst. Growth Des.*, 2013, **13**, 3078-3086.

17 S. J. Ramsden, V. Robins, S. T. Hyde, *Acta Cryst. A*, 2009, **65**, 81; see http://epinet.anu.edu.au/sqc117.

18 (a) ANIDIL: E. Y. Kim, Y. J. Song, H. G. Koo, J. H. Lee, H. M. Park, C. Kim, T.-H. Kwon, S. Huh, S.-J. Kim, Y. Kim, *Polyhedron*, 2010, **29**, 3335; (b) DEGSOY: J. Zhang, Y. Kang, J. Zhang, Z.-J. Li, Y.-Y. Qin, Y.-G. Yao, *Eur. J. Inorg. Chem.*, 2006, **12**, 2253; (c) DEGSOY01: H. S. Huh, S. W. Lee, *J. Mol. Struct.*, 2007, **829**, 44; (d) SIRDOO: J.-J. Wang, T.-T. Wang, L. Tang, X.-Y. Hou, L.-J. Gao, F. Fu, M.-L. Zhang, *J. Coord. Chem.*, 2013, **66**, 3979; (e) TEDDOW: R.-Q. Fang, Y.-F. Zhao, X.-M. Zhang, *Inorg. Chim. Acta*, 2006, **359**, 2023; (f) TEDDOW01: Y. Feng, J. Peng, X. Che, Y. Gao, *J. Coord. Chem.*, 2006, **59**, 1349; (g) VIVDOV: J.-J. Wang, T.-T. Wang, L. Tang, X.-Y. Hou, M.-L. Zhang, L.-J. Gao, F. Fu, Y.-X. Ren, *Z. Anorg. Allg. Chem.*, 2014, **640**, 483.

19 (a) M. Yu, L. Xie, S. Liu, C. Wang, H. Cheng, Y. Ren and Z. Su, *Inorg. Chim. Acta*, 2007, **360**, 3108; (b) E.-C Yang, H.-K Zhao, B. Ding, X.-G. Wang, and X.-J. Zhao, *Cryst. Growth Des.*, 2007, **7**, 2009.